



Efficiently luminescent cuprous iodide complexes supported by novel N[∗]P-chelating ligands: Synthesis, structure and optoelectronic performances

Wei Yang^{a,1}, Weigao Wang^{b,1}, Mengmeng Cao^a, Na Gao^a, Chunmei Liu^a, Jie Zhang^a, Zhengchun Peng^{b,**}, Chenxia Du^{a,***}, Bin Zhang^{a,*}

^a College of Chemistry, Zhengzhou University, Zhengzhou, 450001, PR China

^b Key Laboratory of Optoelectronic Devices and Systems of Ministry of Education and Guangdong Province, College of Physics and Optoelectronic Engineering, Shenzhen University, Shenzhen, Guangdong, 518060, PR China

ARTICLE INFO

Keywords:

N[∗]P chelating ligand
Cuprous complex
Phosphorescence
Organic light emitting diode

ABSTRACT

Phosphorescent cuprous complexes (1–6) with general formula Cu(I)(N[∗]P)(PPh₃), where N[∗]P = 2-(2'-diphenylphosphinophenyl)-1-phenyl-5-methoxybenzimidazole derivatives, have been designed and synthesized. The crystal structures of the neutral four-coordinated Cu(I) complexes are determined by single crystal X-ray diffraction. At 293 K, these complexes exhibit intense phosphorescence with exceptionally high photoluminescence quantum yields (up to 88.3%) and short decay times (4.8–55.2 μs). The emission maxima can be fine-tuned from 529 nm to 577 nm, depending upon the number and position of methoxy substituent on the N[∗]P ligand. Especially, complex 5 exhibits phosphorescence (533 nm) with photoluminescence quantum yield of 70.5% and decay time of 19.5 μs, implying its potential to serve as a phosphor for organic light emitting diode (OLED). Solution-processed OLED incorporating complex 5 as dopant emitter achieves a maximum brightness of 7729 cd with CIE coordinates (0.4351, 0.5398), constituting a step further toward the design of cuprous complexes as cheap and environmental alternatives to the luminescent noble metal complex.

1. Introduction

During the past decade, luminescent copper(I) complexes have caused significant concern because of their fascinating photophysical phenomena and potential applications in newly emerged technologies such as organic light-emitting diode (OLED), information encryption, solar cell, chemical sensor, and bio-imaging [1–9]. Especially, phosphorescent cuprous complexes could harvest both singlet and triplet excitons generated in OLEDs [10,11], which show great potential for industrial application in optoelectronic devices as cheap and environmental alternatives to the luminescent noble metal Ir(III) and Pt(II) complexes [12–14]. Emissive copper(I) complexes have shown to adopt various structural features, including mononuclear [15–18], binuclear [19,20] and multinuclear [21–23] species. Among them, mononuclear copper complexes seem to be considered as an idealized electroluminescent emitters because of their high solubility in organic solvent and vacuum-sublimability [24–27], which is essential for manufacturing

efficient OLEDs.

Most of the mononuclear Cu(I) complexes have a pseudotetrahedral (D_{2d}) geometry, which always undergoes the Jahn-Teller distortion in excited state through metal-to-ligand charge transfer (MLCT) process [28,29]. Such rearrangement usually results in low phosphorescence quantum yield. Recently, phosphine (P)-containing ligands have brought a great breakthrough in the emission efficiency of Cu(I) complexes due to their spatial steric effect as well as strong coordinating ability with the soft acidic Cu(I) ion [30–32]. Specially, considerable attention has been focused on Cu(I) complexes consisting of N[∗]P ligands, as their exceptional structural rigidity and stability could further increase the photoluminescence quantum yield (Φ) [33–36]. However, because the spin-orbit coupling (SOC) parameter (ξ) for Cu nucleus is only 857 cm⁻¹, mononuclear Cu(I) complexes give markedly slow rates intersystem crossing (ISC) processes [37,38]. As a result, copper complexes with high photoluminescence quantum yield as well as short radiative decay time are still rare. It is well known that introducing

* Corresponding author.

** Corresponding author.

*** Corresponding author.

E-mail addresses: zcpeng@szu.edu.cn (Z. Peng), dxc@zsu.edu.cn (C. Du), bz@zsu.edu.cn (B. Zhang).

¹ These authors contributed equally to this work: Wei Yang, Weigao Wang.

heavy atom iodine ($\xi(I) = 5069 \text{ cm}^{-1}$) into molecule can promote the intersystem crossing (ISC) from the singlet to triplet excited state, which could open an efficient short-lived phosphorescence path [39,40]. Meanwhile, the formal oxidation from Cu(I) to Cu(II) upon excitation could be reduced due to the formation of strong Cu–I bond accompanied with iodide-to-copper charge transfer in excited state [41,42]. These facts afford a highly fruitful strategy to prepare efficient phosphorescent materials based on mononuclear Cu(I) complexes.

In the current work, we have designed and synthesized a series of Cu(I) complexes (1–6) with 2-(2'-diphenylphosphinophenyl)-1-phenyl-5-methoxybenzimidazole derivatives (N[∗]P). The bulky N[∗]P chelating ligand and iodine are expected to reduce the non-radiative deactivation process as well as achieve fast radiative rate. Besides, the introduction of methoxy group on the 2-phenyl has a subtle electronic and steric effect, which would slightly tune emission color. Furthermore, as carbazole has profound advantage of hole transport ability and the phosphorescence population [43–45], complexes 4–6 containing carbazole as a sub-structure are synthesized. Indeed, using these strategies, the Cu(I) complexes realized efficient phosphorescence of up to 88.3% with lifetime shorter than 55.2 μs at 293 K. Electroluminescence behaviors with a maximum luminance and current efficiency of 7729 cd m^{-2} and 7.53 cd A^{-1} , respectively, are achieved by a simple solution-processed OLED. The results suggest the possibility of achieving low-cost and high bright OLEDs by using of environmental friendly copper(I) complexes as emitting materials.

2. Results and discussion

2.1. Synthesis

2-(2'-diphenylphosphinophenyl)-1-phenyl-5-methoxybenzimidazole derivatives (N[∗]P) have been prepared according to the synthetic routes involving two-step reactions (Scheme 1) with moderate yields. ¹H NMR, ³¹P NMR and elemental analysis confirm the structures. The copper(I) complexes are obtained by simply adding a stoichiometric amount of CuI, P[∗]N ligand and triphenylphosphine ligand in a CH₃CN–CH₂Cl₂ solvent mixture at room temperature (Scheme 2). The solution mixture affords yellow crystals by slow evaporation solution technique at 298 K. As a result, the species are all isolated as crystals. All the Cu(I) complexes are characterized by single-crystal X-ray diffraction, NMR spectroscopy and elemental analysis.

2.2. Crystal structures of the copper(I) complexes

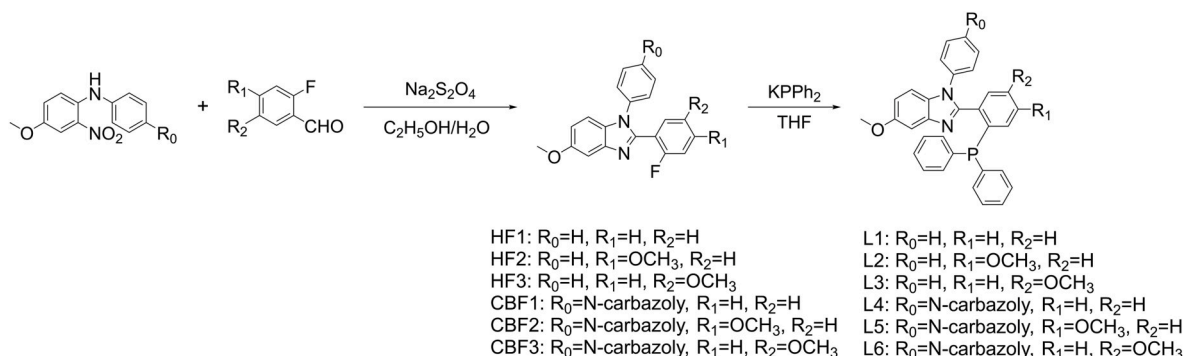
X-ray crystallographic analyses of complexes 1–6 has been carried out to reveal the molecular structures and coordination environments around the Cu(I) atoms. The crystal parameters and refinement data for complexes are shown in Table S1 and Table S2 in the supporting information. ORTEP diagrams of the Cu(I) complexes are illustrated in Fig. 1. Selected bond lengths and angles are summarized in Table S3.

Notably, the N[∗]P ligands, containing different substituents, do not significantly influence the coordination characters: the central Cu⁺ ion is four-coordinated by bidentate P[∗]N ligand, ancillary triphenylphosphine ligand and iodide. Meanwhile, the bond angles of I–Cu–P (PPh₃) range from 106.14 (3)^o to 111.75 (3)^o and N–Cu–P (N[∗]P) range from 86.77 (16)^o to 89.77 (9)^o, which suggest that the monovalent Cu⁺ cations adopt a distorted tetrahedral geometry.

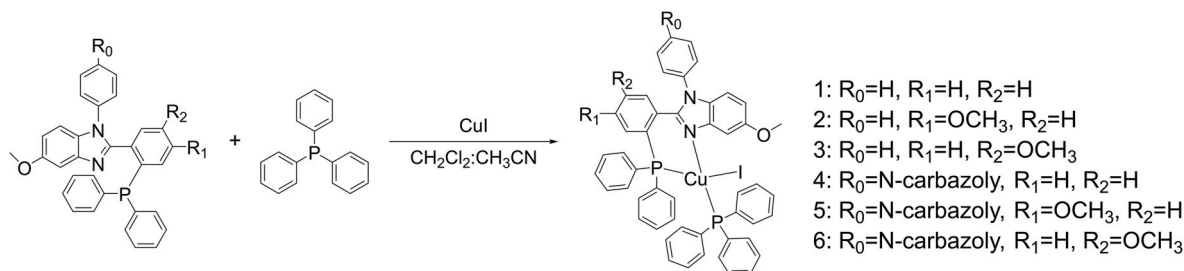
The Cu–I bond lengths are in the range of 2.6173 (4) Å to 2.6440 (5) Å, which are comparable to the values reported for mononuclear Cu(I) complex [24]. Additionally, the P1–Cu1–P2 bond angles are in the ranges of 118.57 (4)^o to 124.32 (4)^o, which are typical for related Cu(I) complexes [46,47]. It is worth noting that the steric hindrance effect and electron effect resulting from the presence of the methoxy group slightly affect the dihedral angles between the 2-benzene ring and the mean plane of benzimidazole in the complexes structure (1: 41.679^o, 2: 44.617^o, 3: 42.943^o). As a result, the N–Cu–P (N[∗]P) bond angles are 89.09 (8)^o, 89.45 (9)^o and 87.98 (7)^o, which suggest that the order of increasing distortion from idealized tetrahedral geometry is 2 < 1 < 3. Meanwhile, the methoxy substituents result in shorter Cu1–P1 bond lengths (2: 2.2853 (11) Å and 3: 2.2696 (8) Å) than that of 1 (2.2944 (9) Å). In addition, the introduction of carbazole moiety exerts some steric hindrance effect, which lead to slightly decreased dihedral angles between the 2-benzene ring and benzimidazole moiety: 36.377^o for 4, 40.036^o for 5 and 37.643^o for 6. Obviously, the dihedral angle of 5 decrease slightly less (4.581^o) than those of the others (5.302^o for 4 and 5.3^o for 6), comparing with the dihedral angle of the corresponding 2, 1 and 3, respectively. Consequently, the Cu1–P1 distances increase in the following order: 6 (2.2674 (17) Å) < 4 (2.2698 (8) Å) < 5 (2.2805 (10) Å), which do not follow the same trend of the complexes without carbazole substituent (3 < 2 < 1). The bite angles N–Cu–P (N[∗]P) suggest that the distortion degree of the geometry slightly increase in the order of 5 < 4 < 6. The distortion degree of the geometries suggest that photoluminescence quantum yields of 2 and 5 would be higher than those of the others. As illustrated in Fig. S1 in the supporting information, crystal packing of the complexes exhibit only partially overlapping between the aromatic rings with a separation of more than 3.7 Å (1, 2, 4 and 5), which rules out any significant π – π interactions between the molecules [14,48]. Obviously, these phenomena could be ascribing to the rigid structure and large steric hindrance of the N[∗]P ligands.

2.3. Photophysical properties and theoretical calculations

The UV/Vis absorption spectra of P[∗]N ligands and Cu(I) complexes 1–6 are investigated in CH₂Cl₂ solution at ambient temperature. The absorption maxima (λ_{abs}) and the related molar extinction coefficients (ϵ) are summarized in Table S4. Due to the structural similarity, all complexes show similar ligand-centered transitions. The absorption spectra of complex 2 and 5 together with their corresponding free ligands are shown in Fig. 2 and discussed as a representative example, while the spectra of others can be found in Fig. S2 and Fig. S3 in the



Scheme 1. Synthetic Procedures for Ligands.



Scheme 2. Synthetic Procedures for Cu(I) Complexes 1-6.

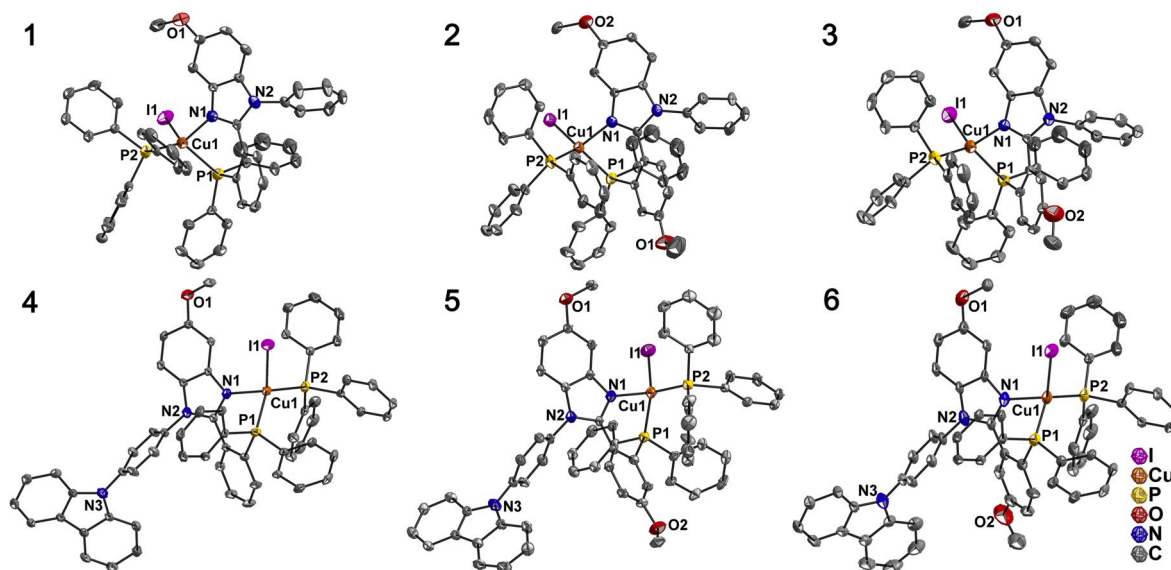


Fig. 1. ORTEP drawing of the complexes with ellipsoids at the 30% probability level. Hydrogen atoms are omitted for clarity.

supporting information.

Both complexes display similar intense absorption bands in the lower wavelength range up to ca. 240 nm with molar absorption coefficient (ϵ) more than $5 \times 10^4 \text{ M}^{-1} \text{ cm}^{-1}$, which can be assigned to the spin allowed intraligand charge transfer (ILCT) transitions localized on the N'P and PPh₃ ligands. They are followed by a slow decline at around 260 nm, which are also considered as the typical π -electron response of the ligands. The broad shoulders at about 307 nm (for 2) and 309 nm (for 5) with $\epsilon > 1 \times 10^4 \text{ M}^{-1} \text{ cm}^{-1}$ exhibit slightly red-shifted features compared to that of the relative free N'P ligand, which suggest these moderate absorptions could be attributed to the predominant ILCT transitions within N'P ligand mixed with some metal-to-ligand charge transfer (MLCT) and halide-to-ligand charge transfer (XLCT). Notably, complex 5 exhibits structured absorption bands between 290 and 380 nm, which could be attributed to allowed transitions within the

carbazole moiety [49–51]. Similar phenomena are also observed in the absorption spectra of 4 and 6. Moreover, broad and weak low-energy absorption tails over 350 nm, which are not observed in the corresponding free ligands spectra, which might be attributed to the charge transfer transitions including MLCT and XLCT transitions.

The assignment of absorptions at long wavelengths over 260 nm is further supported by the density functional theory (DFT) and time-dependent density functional theory (TDDFT) calculations at B3LYP/LANL2DZ (Cu, I)/6-31G** (C, H, N, O, P) level. The optimized structures in the ground state (S_0) correlate well to the X-ray structures (Fig. S4 and Table S5), which ensure the accuracy of DFT studies. The calculated low energy absorptions of complexes 2 and 5 are showed in Fig. 2b and c, respectively. The relative data are summarized in Table S6 and Table S7. The calculated results for the other complexes are shown in Fig. S2, Fig. S3, Table S6 and Table S7.

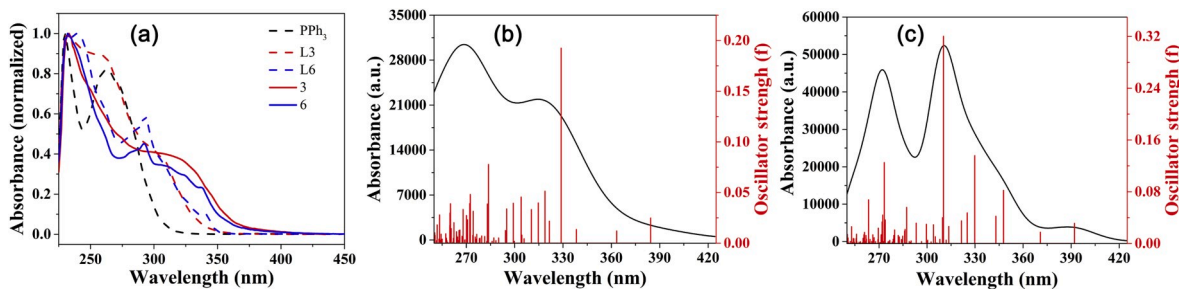


Fig. 2. (a) UV-vis absorption spectra of 2 and 5 together with the corresponding free ligands in CH_2Cl_2 solution ($1 \times 10^{-5} \text{ M}$) at room temperature. Simulated absorption spectra with vertical excitation energies and oscillator strengths for 2 and 5 are depicted in (b) and (c), respectively.

According to the calculation, the absorption onsets at lower energies after 350 nm can be ascribed to the electronic transitions of highest occupied molecular orbital (HOMO, H) to lowest unoccupied molecular orbital (LUMO, L) and HOMO-1 to LUMO (Fig. 3, Fig. S5 and Table S6). On the basis of the orbital compositions analysis (Table S8), it can be seen that the iodide, copper ion and N⁺P ligand contribute significantly to the HOMO and HOMO-1. Meanwhile, HOMO-1 is also distributed over the PPh₃ ligand. On the other hand, the LUMO of the complexes is mainly localized on the N⁺P ligand (>95%). Consequently, the absorption tails (>350 nm) of the complexes in experiment can reasonably be assigned to a predominantly mixture of MLCT and XLCT transitions together with some contributions of ligand (PPh₃)-to-ligand (N⁺P) charge transfer (LLCT) transition. Furthermore, the HOMO-LUMO energy gaps of these complexes are affected by the substitutions on the N⁺P ligands, which increase in the order of $6 < 4 < 1 < 3 < 2 < 5$.

Besides, the calculated strong absorptions of the complexes, ranging between 260 nm and 350 nm, are in good agreement with the experimental results. The calculated absorption bands peaking at 265–275 nm are consistent with the observed in the UV spectra as an additional shoulder located in ca.260 nm. The lower energy electronic transitions occurring at 300–350 nm agree well with the broad shoulders appeared at 285–350 nm in experiment, are mainly N⁺P ligand-centered ILCT in nature together with some contributions of MLCT and XLCT.

All the complexes in powder show bright luminescence with maxima (λ_{em}) from 529 to 577 nm at 293 K when they are excited under the wavelengths of excitation maxima (λ_{ex}) (Fig. 4 and Table 1). The broad without vibronic progression emission spectra imply that the luminescence generates from charge-transfer (CT) state involving MLCT and XLCT, which has been widely observed previously in related Cu(I) iodine complexes [52,53]. As expectedly, the methoxy substitutions play an interesting role in tuning the luminescent wavelengths: the emission maxima of complex 2 (529 nm) bearing 4'-methoxy group shows a significantly blue shift of 1014 cm^{-1} compared with that of complex 1 (559 nm), while complexes 3 (556 nm) with 5'-methoxy group only exhibits a slightly blue shift (96 cm^{-1}) in luminescence relative to 1 (559 nm). Similar phenomena have also been found in the carbazole substituted complexes 5 (533 nm) < 6 (564 nm) < 4 (577 nm), suggesting that the methoxy group could finely tune the emission peaks of the complexes. Furthermore, comparing emission spectra between 1 and 4, 2 and 5, 3 and 6, it is found that the carbazole substitution results in a slightly red shift of emission maxima. The relative ordering of the emission energies correlates well with the HOMO-LUMO gaps in the absorption spectra. Importantly, all the complexes present high photoluminescent quantum yields (Φ) from 31.1% to 88.3%, especially for complex 2 (88.3%) and 5 (70.5%). Additionally, 2 and 5 are endowed with larger radiative decay rate (K_r) than non-radiative decay rate (K_{nr}),

justifying their high photoluminescent quantum yields.

The luminescence lifetimes (τ_{obs}) of the complexes have proved to be single exponential in the range of 4.8–55.2 μs at 293 K (Fig. S6 and Fig. S7), confirming the strong spin-orbit coupling (SOC) mediated by the heavy atoms (Cu and I). On the basis of the microsecond photoluminescence decay times and large Stokes shifts (6207–9892 cm^{-1}), the emissions of the complexes are probably assigned as phosphorescence involving MLCT and XLCT state [54–56]. Furthermore, the emission maxima of the complexes are slightly blue-shifted when cooling from 293 K to 77 K, as similarly reported for related Cu(I) complexes, which are possibly due to the ground state of the Cu(I) complex is more stabilized in energy at low temperature [57,58]. Simultaneously, the luminescent decay kinetics of complexes reveal the lifetimes at 77 K are also in the microsecond range, which are only 1–6 times longer than that at 293 K (Table 1). These temperature-dependent behaviors demonstrate that the photoluminescence of 1–6 arises from triplet charge transfer (³CT) state [57,59]. Notably, complex 5 shows phosphorescence with a high Φ of 70.5% and a short decay time (19.5 μs), which is comparable to those of phosphorescent emitters with noble metals, demonstrating its potential optoelectronic applications.

2.4. Electroluminescent properties

Impelled by the outstanding advantages of complex 5, doped OLEDs are fabricated by hybrid solution-processing method to evaluate the electroluminescent (EL) properties of 5. The bottom-emitting device structure is configured as follows: glass/ITO/PEDOT:PSS (40 nm)/x wt % 5: CBP (30 nm)/TPBI (40 nm)/LiF (1 nm)/Al (150 nm). In the device configuration, PEDOT: PSS (poly (3,4-ethylenedioxythiophene): poly (styrenesulfonate)) serves the function of hole-transporting material, CBP (4,4'-bis(carbazole-9-yl)biphenyl) acts as the host material for the phosphorescent emitter, TPBI (1,3,5-tris(N-phenylbenzimidazole-2-yl)benzene) is employed as the electron transport material, and LiF plays the role of electron injection. Additionally, in order to understand the effect of 5 doping concentrations on OLED performance, four OLEDs with 5 concentrations of 5 wt% (device A), 10 wt% (device B), 20 wt% (device C) and 40 wt% (device D) are designated. The EL characteristics of every device are depicted in Fig. 5, and the data are summarized in Table 2.

The profiles of EL spectra of the devices A-D are nearly identical with an emission maximum at 558 nm, which are red-shifted (841 cm^{-1}) with respect to the PL spectrum in powder. It is commonly acknowledged that the minor shifts is likely due to "solvent" effects of the host matrices [12, 60]. But closer inspection of the CIE1931 coordinates (Table 2) indicates that the electroluminescence color is slightly red-shifted, which could be explained by the combination of aggregation and solvation effects [49].

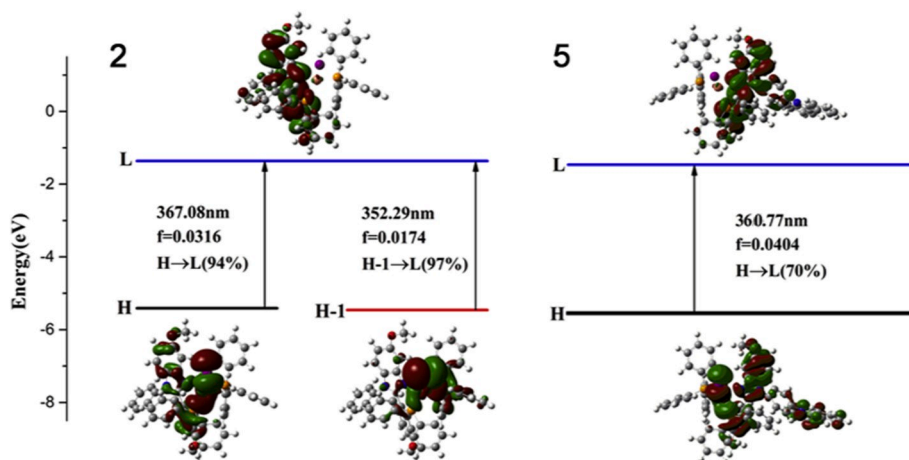


Fig. 3. The calculated low-energy transitions for 2 and 5 and the relative frontier molecular orbitals (contributions > 25%).

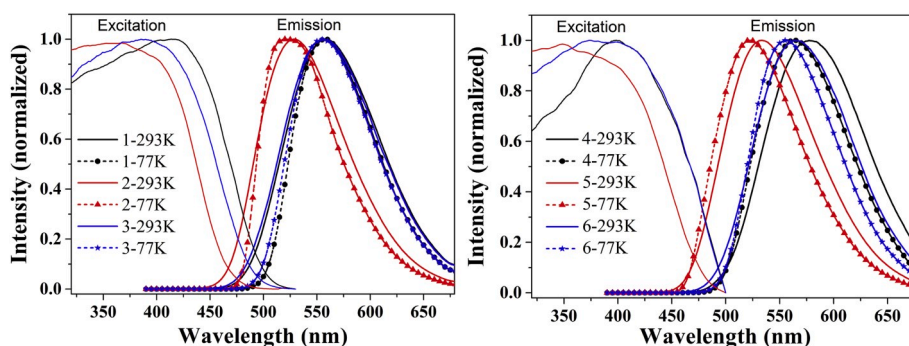


Fig. 4. Normalized excitation and emission spectra of complexes 1–6 in powder at 293 K and the normalized photoluminescence spectra of the complexes at 77 K.

Table 1

Photophysical data for the Cu(I) complexes in powder.

Complex	T = 293 K						T = 77 K	
	$\lambda_{\text{ex}}/\text{nm}$	$\lambda_{\text{em}}/\text{nm}$	$\tau_{\text{obs}}/\mu\text{s}$	$\Phi/\%$	$K_{\text{r}}a/10^4 \text{ s}^{-1}$	$K_{\text{nr}}b/10^4 \text{ s}^{-1}$	$\lambda_{\text{em}}/\text{nm}$	$\tau_{\text{obs}}/\mu\text{s}$
1	415	559	14.2	41.7	2.95	4.12	558	32.5
2	368	529	55.2	88.3	1.60	0.21	521	75.0
3	390	556	12.8	31.1	2.43	5.40	555	33.7
4	400	577	4.8	41.3	8.66	12.30	564	27.8
5	349	533	19.5	70.5	1.21	0.50	522	58.5
6	376	564	10.5	34.6	3.30	6.23	556	39.0

^a $k_{\text{r}} = \Phi/\tau_{\text{obs}}$

^b $k_{\text{nr}} = 1/\tau_{\text{obs}} - k_{\text{r}}$

Additionally, no emission from the host material or other organic layers is detected as well as the maximum emissions are stable under different driving voltages, implying that energy transfer from the CBP to 5 is sufficient.

The current density (J)-voltage-luminescence characteristics of the devices demonstrate that the turn-on voltages (recorded at a luminance of 1 cd m^{-2}) are similar (ca. 5.6 V). By comparing four devices, it is found that the device A has achieved the relatively higher EL performance, which gives a maximum brightness of 7729 cd m^{-2} at 13.8 V, a peak current efficiency (CE) of 7.53 cd A^{-1} and a maximum external quantum efficiency (EQE) of 2.38% (Table 2). Obviously, despite the high brightness, the efficiencies of the OLED based on 5 are undesirable, especially compared with the pretty good photoluminescent quantum yield, which may be caused by the geometry rearrangement at excited state of 5 in the host. On the other hand, an interesting finding is that the devices with different doping concentrations (5%–40%) exhibit only a minor decrease in the efficiency and nearly identical electroluminescence color, suggesting that the molecule are favorable for OLED applications.

3. Conclusions

A series of luminescent Cu(I) iodide complexes (1–6) of general formula $\text{Cu}(\text{N}^{\text{P}})(\text{PPh}_3)$ have been designed and fabricated. At 293 K, all complexes in powder exhibit broad and featureless emission bands with peak maxima in the range 529–577 nm, which show that the introduction of methoxy substitution could fine-tune the luminescent wavelengths. Meanwhile, the photophysical behavior of these complexes at 293 K and 77 K demonstrates that they are typical phosphorescence material. Notably, the combined effects of strong coordinating ability (N^{P} and I) and the synergistic heavy atom effects (I and Cu) of the complexes (1–6) result in highly efficient phosphorescence with photoluminescence quantum yields of 41.7%, 88.3%, 31.1%, 41.3%, 70.5% and 34.6% at short emission decay times (τ) of 14.2 μs , 55.2 μs , 12.8 μs , 4.8 μs , 19.5 μs and 10.5 μs , respectively, which support the proposed design strategy. Bright electroluminescence of up to 7729 cd m^{-2} has been observed based on phosphor 5 as dopant in a simple solution-processed OLED. Although the devices with different doping concentrations (5%–40%) exhibited inferior efficiency, high brightness ($>6500 \text{ cd m}^{-2}$) as well as nearly consist emission color and efficiency

Table 2

EL performances of devices with complex 5.

Device	$\lambda_{\text{EL}}/\text{nm}$	$L_{\text{max}}^{\text{a}}/\text{cd m}^{-2}$	$\text{CE}_{\text{max}}^{\text{b}}/\text{cd A}^{-1}$	$\text{EQE}_{\text{max}}^{\text{c}}/\%$	CIE1931 (x, y)
A	558	7729	7.53	2.38	(0.4351, 0.5398)
B	558	7724	6.68	2.12	(0.4387, 0.5378)
C	558	6846	6.82	2.19	(0.4426, 0.5350)
D	558	5671	7.25	2.35	(0.4439, 0.5338)

^a Maximum luminance.

^b Maximum CE.

^c Maximum EQE.

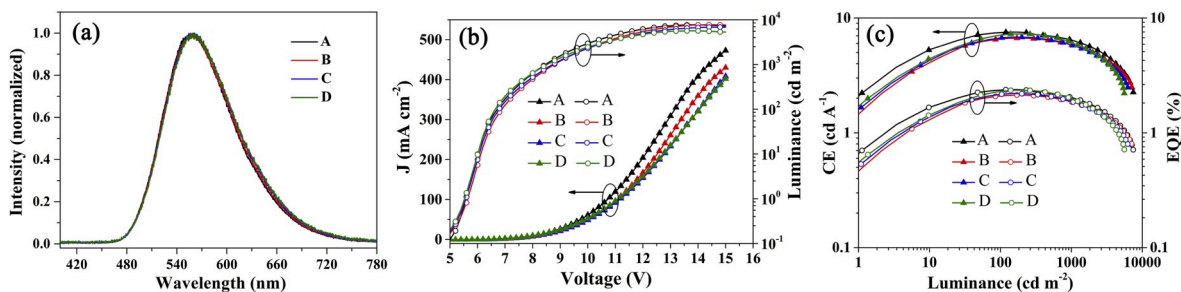


Fig. 5. (a) EL spectra for the devices. (b) Current density (J)-Voltage-Luminescence characteristics. (c) Current Efficiency (CE)-Luminance and external quantum efficiency (EQE)-Luminance characteristics.

are observed. These encouraging results manifest highly efficient electroluminescence could be expected for this kind of cuprous complexes by further strengthening the rigidity of the molecular structure to decreasing the non-radiative transitions in doped OLEDs.

4. Experimental section

4.1. Methods

The solvents tetrahydrofuran (THF), acetonitrile (CH₃CN) and dichloromethane (CH₂Cl₂) were freshly distilled from appropriate drying agents prior to use. All other commercially available solvents and reagents were used as received. All air and moisture sensitive reactions were carried out under an argon atmosphere with standard vacuum line techniques. ¹H NMR and ³¹P NMR spectra were measured on a Bruker 400 MHz NMR spectrometer. Elemental analyses for C, H, and N were carried out by employing Vario EL III Elemental Analyzer. UV-vis absorption spectra were acquired on a Varian Cary 5000 UV-vis-NIR spectrophotometer. Steady state excitation and emission spectra, photoluminescent lifetime as well as the absolute quantum efficiency of the complexes were collected by Edinburgh Instruments FLS980 spectrometer.

4.2. Synthesis

4.2.1. Synthesis of ligands

Synthesis of HF1. 4-methoxy-2-nitrodiphenylamine (18.0 mmol, 4.40 g) and 2-fluorobenzaldehyde (19.1 mmol, 2.37 g) were dissolved in 5:1 C₂H₅OH/H₂O mixture. Na₂S₂O₄ (90.0 mmol, 15.67 g) was added to the solution, and then the mixture was stirred at 75 °C for 5 h. After cooling, the mixture was poured into water, and extracted with ethyl acetate. The organic solvent was removed under reduced pressure to give a brown oil. The crude product was purified by column chromatography with hexane/ethyl acetate as eluent to afford the sample as a white powder (yield: 4.0 g, 70%) ¹H NMR (400 MHz, CDCl₃) δ 7.65 (td, *J* = 7.4, 1.8 Hz, 1H), 7.46–7.35 (m, 5H), 7.26–7.17 (m, 4H), 7.00–6.93 (m, 2H), 3.91 (s, 3H). Anal. Calcd/%: C, 75.46; H, 4.75; N, 8.80. Found: C, 75.40; H, 4.73; N, 8.83.

Synthesis of HF2. This compound was prepared by using the method described for the synthesis of HF1. Yield 75%. ¹H NMR (400 MHz, CDCl₃) δ 7.54 (t, *J* = 8.4 Hz, 1H), 7.48–7.34 (m, 4H), 7.25–7.18 (m, 3H), 6.93 (dd, *J* = 8.8, 2.4 Hz, 1H), 6.74 (dd, *J* = 8.6, 2.4 Hz, 1H), 6.50 (dd, *J* = 11.9, 2.4 Hz, 1H), 3.90 (s, 3H), 3.80 (s, 3H). Anal. Calcd/%: C, 72.40; H, 4.92; N, 8.04. Found: C, 72.47; H, 4.93; N, 8.02.

Synthesis of HF3. This compound was prepared by using the method described for the synthesis of HF1. Yield 74%. ¹H NMR (400 MHz, CDCl₃) δ 7.47–7.36 (m, 4H), 7.27 (d, *J* = 1.6 Hz, 1H), 7.24 (d, *J* = 8.9 Hz, 2H), 7.15 (dd, *J* = 5.4, 2.9 Hz, 1H), 6.95 (dd, *J* = 8.9, 2.4 Hz, 1H), 6.93–6.82 (m, 2H), 3.90 (s, 3H), 3.77 (s, 3H). Anal. Calcd/%: C, 72.40; H, 4.92; N, 8.04. Found: C, 72.37; H, 4.91; N, 8.06.

Synthesis of CBF1. This compound was prepared by using the method described for the synthesis of HF1. Yield 65%; ¹H NMR (400 MHz, CDCl₃) δ 8.15 (d, *J* = 7.7 Hz, 2H), 7.76 (td, *J* = 7.4, 1.7 Hz, 1H), 7.66–7.62 (m, 2H), 7.52–7.37 (m, 9H), 7.35–7.26 (m, 3H), 7.10–6.99 (m, 2H), 3.93 (s, 3H); Anal. Calcd/%: C, 79.49; H, 4.59; N, 8.69; Found: C, 79.57; H, 4.59; N, 8.67.

Synthesis of CBF2. This compound was prepared by using the method described for the synthesis of HF1. Yield 60%; ¹H NMR (400 MHz, CDCl₃) δ 8.16 (d, *J* = 7.7 Hz, 2H), 7.70–7.60 (m, 3H), 7.52–7.47 (m, 2H), 7.46–7.42 (m, 4H), 7.41–7.29 (m, 4H), 7.00 (dd, *J* = 8.9, 2.4 Hz, 1H), 6.82 (dd, *J* = 8.6, 2.4 Hz, 1H), 6.58 (dd, *J* = 11.9, 2.4 Hz, 1H), 3.93 (s, 3H), 3.84 (s, 3H); Anal. Calcd/%: C, 77.18; H, 4.71; N, 8.18; Found: C, 77.06; H, 4.69; N, 8.20.

Synthesis of CBF3. This compound was prepared by using the method described for the synthesis of HF1. Yield 63%; ¹H NMR (400 MHz, CDCl₃) δ 8.15 (d, *J* = 7.7 Hz, 2H), 7.67–7.62 (m, 2H), 7.53–7.48

(m, 2H), 7.46–7.37 (m, 6H), 7.34–7.29 (m, 2H), 7.28–7.26 (m, 1H), 7.03 (dd, *J* = 8.9, 2.4 Hz, 1H), 6.98–6.93 (m, 2H), 3.93 (s, 3H), 3.83 (s, 3H); Anal. Calcd/%: C, 77.18; H, 4.71; N, 8.18; Found: C, 77.23; H, 4.72; N, 8.16.

Synthesis of L1. A mixture of HF1 (1.59 g, 5.00 mmol) and potassium diphenylphosphide (10.5 ml, 0.5 M in THF, 5.25 mmol) in dry THF (20 ml) was refluxed under argon atmosphere for 24 h. After cooling to room temperature, the THF was removed under reduced pressure. CH₃OH (35 ml) was added to the residue, affording a white precipitate. The final product was re-crystallized from CH₂Cl₂/CH₃OH solution and dried under vacuum at 40 °C for 5 h. Yield: 1.75 g, 72%. ¹H NMR (400 MHz, CDCl₃) δ 7.55–7.50 (m, 1H), 7.40–7.26 (m, 4H), 7.25–7.16 (m, 11H), 7.11–7.07 (m, 1H), 7.02–6.96 (m, 4H), 6.92 (dd, *J* = 8.8, 2.4 Hz, 1H), 3.88 (s, 3H). ³¹P NMR (162 MHz, CDCl₃) δ –12.94 (s). Anal. Calcd/%: C, 79.32; H, 5.20; N, 5.78. Found: C, 79.35; H, 5.19; N, 5.76.

Synthesis of L2. This compound was prepared by using the method described for the synthesis of L1. Yield 69%; ¹H NMR (400 MHz, CDCl₃) δ 7.42 (dd, *J* = 8.5, 4.1 Hz, 1H), 7.32–7.26 (m, 4H), 7.25–7.14 (m, 9H), 7.02 (td, *J* = 7.6, 1.7 Hz, 4H), 6.92–6.85 (m, 2H), 6.60–6.55 (m, 1H), 3.88 (s, 3H), 3.63 (s, 3H). ³¹P NMR (162 MHz, DMSO) δ –13.71 (s). Anal. Calcd/%: C, 77.03; H, 5.29; N, 5.44. Found: C, 77.10; H, 5.28; N, 5.42.

Synthesis of L3. This compound was prepared by using the method described for the synthesis of L1. Yield 65%; ¹H NMR (400 MHz, CDCl₃) δ 7.31 (d, *J* = 2.4 Hz, 1H), 7.25–7.15 (m, 12H), 7.12 (t, *J* = 2.9 Hz, 1H), 7.00 (dd, *J* = 8.6, 3.3 Hz, 1H), 6.96–6.86 (m, 6H), 3.89 (s, 3H), 3.78 (s, 3H). ³¹P NMR (162 MHz, CDCl₃) δ –15.19 (s). Anal. Calcd/%: C, 77.03; H, 5.29; N, 5.44. Found: C, 77.15; H, 5.27; N, 5.43.

Synthesis of L4. This compound was prepared by using the method described for the synthesis of L1. Yield 78%; ¹H NMR (400 MHz, CDCl₃) δ 8.16 (d, *J* = 8.5 Hz, 2H), 7.68–7.63 (m, 1H), 7.58–7.53 (m, 2H), 7.48–7.36 (m, 9H), 7.35–7.29 (m, 3H), 7.23–7.16 (m, 6H), 7.15–7.11 (m, 1H), 7.07–6.97 (m, 5H), 3.91 (s, 3H). ³¹P NMR (162 MHz, CDCl₃) δ –12.44 (s). Anal. Calcd/%: C, 81.34; H, 4.96; N, 6.47. Found: C, 81.26; H, 4.98; N, 6.46.

Synthesis of L5. This compound was prepared by using the method described for the synthesis of L1. Yield 72%; ¹H NMR (400 MHz, CDCl₃) δ 8.17 (d, *J* = 7.7 Hz, 2H), 7.61–7.53 (m, 3H), 7.49–7.40 (m, 6H), 7.38–7.28 (m, 4H), 7.24–7.17 (m, 6H), 7.10–7.02 (m, 4H), 7.00–6.94 (m, 2H), 6.63–6.59 (m, 1H), 3.90 (s, 3H), 3.67 (s, 3H). ³¹P NMR (162 MHz, CDCl₃) δ –11.27 (s). Anal. Calcd/%: C, 79.51; H, 5.04; N, 6.18. Found: C, 79.45; H, 5.06; N, 6.17.

Synthesis of L6. This compound was prepared by using the method described for the synthesis of L1. Yield 75%; ¹H NMR (400 MHz, CDCl₃) δ 8.17 (d, *J* = 7.7 Hz, 2H), 7.60–7.54 (m, 2H), 7.52–7.47 (m, 2H), 7.46–7.38 (m, 5H), 7.35–7.30 (m, 3H), 7.24 (t, *J* = 3.0 Hz, 1H), 7.20–7.13 (m, 6H), 7.07–6.93 (m, 7H), 3.91 (s, 3H), 3.84 (s, 3H). ³¹P NMR (162 MHz, CDCl₃) δ –14.64 (s). Anal. Calcd/%: C, 79.51; H, 5.04; N, 6.18. Found: C, 79.60; H, 5.02; N, 6.20.

4.2.2. Synthesis of cuprous complexes

General Procedure. Upon stirring, a solution of CuI (1.0 mmol) in CH₃CN (10 ml) was added to a solution of N³P ligand (1.05 mmol) in CH₃CN (15 ml)/CH₂Cl₂ (15 ml). Then, PPh₃ (1.02 mmol) was added to the solution, and the reaction mixture was stirred for 1.5 h at room temperature. The resultant solution was left unperturbed for ca. 2–3 weeks at 298 K until a lot of yellow crystals emerged. The afforded products were isolated by filtration, washed with small amounts of CH₃CN/CH₂Cl₂ (1:1) and dried under vacuum at 50 °C. Yields: 43–70% (based on Cu).

Complex 1 (C₅₀H₄₀N₂OP₂CuI): yield: 51%. ¹H NMR (400 MHz, CDCl₃) δ 8.17 (d, *J* = 2.4 Hz, 1H), 7.47 (t, *J* = 8.6 Hz, 7H), 7.40–7.27 (m, 10H), 7.24–7.06 (m, 14H), 7.03 (t, *J* = 7.3 Hz, 1H), 6.98–6.93 (m, 2H), 6.92 (s, 1H), 6.82 (dd, *J* = 8.9, 2.4 Hz, 1H), 3.71 (s, 3H); ³¹P NMR (162 MHz, CDCl₃) δ –4.12 (s), –17.61 (s). Anal. Calcd/%: C, 64.07; H, 4.30; N, 2.99. Found: C, 64.16; H, 4.29; N, 2.98.

Complex **2** (C₅₁H₄₂N₂O₂P₂CuI): yield: 60% ¹H NMR (400 MHz, CDCl₃) δ 8.18 (s, 1H), 7.48 (t, *J* = 7.8 Hz, 8H), 7.41–7.27 (m, 10H), 7.19 (t, *J* = 6.7 Hz, 11H), 6.94–6.77 (m, 4H), 6.57 (dd, *J* = 8.7, 2.7 Hz, 1H), 6.50 (dd, *J* = 7.4, 2.6 Hz, 1H), 3.71 (s, 3H), 3.57 (s, 3H); ³¹P NMR (162 MHz, CDCl₃) δ –3.91 (s), –16.95 (s). Anal. Calcd/%: C, 63.33; H, 4.38; N, 2.90. Found: C, 63.41; H, 4.37; N, 2.91.

Complex **3** (C₅₁H₄₂N₂O₂P₂CuI): yield: 70% ¹H NMR (400 MHz, CDCl₃) δ 8.18 (d, *J* = 2.1 Hz, 1H), 7.49 (t, *J* = 8.6 Hz, 7H), 7.39 (s, 4H), 7.29 (t, *J* = 6.9 Hz, 7H), 7.17 (t, *J* = 6.9 Hz, 11H), 6.97–6.78 (m, 4H), 6.72 (dd, *J* = 8.6, 2.5 Hz, 1H), 6.51–6.44 (m, 1H), 3.69 (s, 3H), 3.39 (s, 3H); ³¹P NMR (162 MHz, CDCl₃) δ –4.25 (s), –18.58 (s). Anal. Calcd/%: C, 63.33; H, 4.38; N, 2.90. Found: C, 63.26; H, 4.36; N, 2.91.

Complex **4** (C₆₂H₄₇N₃O₂P₂CuI): yield: 43% ¹H NMR (400 MHz, CDCl₃) δ 8.24 (d, *J* = 2.0 Hz, 1H), 8.16 (d, *J* = 7.7 Hz, 2H), 7.59–7.41 (m, 11H), 7.38–7.26 (m, 12H), 7.25–7.14 (m, 11H), 7.14–7.03 (m, 5H), 6.91 (dd, *J* = 8.9, 2.4 Hz, 2H), 3.75 (s, 3H); ³¹P NMR (162 MHz, CDCl₃) δ –3.94 (s), –17.75 (s). Anal. Calcd/%: C, 67.55; H, 4.30; N, 3.81. Found: C, 67.50; H, 4.31; N, 3.81.

Complex **5** (C₆₃H₄₉N₃O₂P₂CuI): yield: 65% ¹H NMR (400 MHz, CDCl₃) δ 8.24 (d, *J* = 1.8 Hz, 1H), 8.16 (d, *J* = 7.7 Hz, 2H), 7.61–7.41 (m, 12H), 7.40–7.27 (m, 11H), 7.20 (t, *J* = 7.1 Hz, 10H), 7.08 (d, *J* = 8.9 Hz, 2H), 6.99 (dd, *J* = 8.6, 4.5 Hz, 2H), 6.89 (dd, *J* = 8.9, 2.4 Hz, 1H), 6.71 (dd, *J* = 8.7, 2.7 Hz, 1H), 6.57 (dd, *J* = 7.3, 2.6 Hz, 1H), 3.74 (s, 3H), 3.62 (s, 3H); ³¹P NMR (162 MHz, CDCl₃) δ –4.12 (s), –17.31 (s). Anal. Calcd/%: C, 66.82; H, 4.36; N, 3.71. Found: C, 66.83; H, 4.37; N, 3.70.

Complex **6** (C₆₃H₄₉N₃O₂P₂CuI): yield: 56% ¹H NMR (400 MHz, CDCl₃) δ 8.24 (d, *J* = 2.1 Hz, 1H), 8.16 (d, *J* = 7.7 Hz, 2H), 7.60 (d, *J* = 7.9 Hz, 2H), 7.55–7.41 (m, 10H), 7.38–7.27 (m, 11H), 7.19 (t, *J* = 7.2 Hz, 10H), 7.12 (d, *J* = 8.9 Hz, 2H), 7.00–6.89 (m, 3H), 6.80 (dd, *J* = 8.6, 2.6 Hz, 1H), 6.61–6.56 (m, 1H), 3.73 (s, 3H), 3.57 (s, 3H); ³¹P NMR (162 MHz, CDCl₃) δ –4.31 (s), –19.03 (s). Anal. Calcd/%: C, 66.82; H, 4.36; N, 3.71. Found: C, 66.75; H, 4.34; N, 3.72.

4.3. Single crystal X-ray crystallography

The diffraction data for **1–4** were collected on an Oxford Xcalibur four-circle diffractometer using graphite-monochromatized Mo-*K*α (λ = 0.71073 Å) and Cu-*K*α (λ = 1.54178 Å) radiation for **1–3** and **4**, respectively. The X-ray diffraction data for **5** and **6** were performed on a Rigaku XtaLAB Pro four-circle diffractometer with Cu-*K*α radiation (λ = 1.54184 Å). Data collection and reduction were processed using the program CrysAlisPro [61]. The crystal structures of **1–6** were solved by direct methods using SHELXS [62] within Olex2 GUI [63], and the non-hydrogen atoms were refined anisotropically by full-matrix least-squares method on F² with SHELXL program [64]. All hydrogen atoms were placed in calculated positions and refined in a riding model along with attached atoms. CCDC 1978807–1978,812 contain the supplementary crystallographic data for the complexes, which can be obtained free of charge from The Cambridge Crystallographic Data Centre via www.ccdc.cam.ac.uk/data_request/cif.

4.4. Theoretical calculations

All the calculations were performed using the Gaussian 09 program package [65]. The geometries obtained from the X-ray diffraction studies served as the initial structures for the optimization. The molecules in the electronic ground state (S₀) were fully optimized without symmetry constraint using density functional theory (DFT) method with B3LYP hybrid exchange correlation functional [66–70]. Time-dependent DFT (TD-DFT) calculations were performed on the subsequent structures using the same method to understand the absorption transition. In these calculations, a “double- ζ ” quality basis set (LANL2DZ) was employed to describe the Cu and I atoms [71,72], and the other atoms C, H, O, N and P are described by 6–31G** [73,74]. Visualization of the optimized structures and frontier molecular orbitals were obtained by GaussView 5.0 program. The simulated absorption

spectra were supported by using the Multiwfn 3.4.1 program [75].

4.5. Fabrication and characterization of OLEDs

Indium-tin-oxide (ITO) coated glass substrates with a sheet resistance of 20 Ω per square were thoroughly cleaned and treated with UV-zone before use. PEDOT:PSS was spin-coated onto the ITO substrate at a speed of 3000 rpm, and then the substrate was annealed at 120 °C for 20 min in an oven. After the substrate was cooled to room temperature, **5** and CBP in chlorobenzene solution was filtered through 0.25 μm pore filter and then overlaid by spin coating on the substrate at 2000 rpm. The sample was transferred to a vacuum evaporation system. The other layers were deposited onto the substrates by thermal evaporation under a high vacuum (<5 × 10^{−4} Pa). The electroluminescence spectra and CIE coordinates were performed by PR650 spectra scan spectrometer. The current density and luminance versus driving voltage characteristics were carried out on a programmable source meter (Keithley 2614B). Current efficiency (CE) and External quantum efficiency (EQE) were calculated based on the current density (*J*)-voltage-luminescence characteristic and EL spectrum.

Declaration of competing interest

The authors declare that they have no known competing financial interests or personal relationships that could have appeared to influence the work reported in this paper.

CRediT authorship contribution statement

Wei Yang: Methodology, Formal analysis, Data curation, Validation, Writing - original draft. **Weigao Wang:** Methodology, Formal analysis, Data curation, Validation, Writing - original draft. **Mengmeng Cao:** Methodology, Formal analysis, Data curation, Validation. **Na Gao:** Methodology, Formal analysis, Data curation, Validation. **Chunmei Liu:** Methodology, Formal analysis, Data curation, Validation, Software, Visualization. **Jie Zhang:** Software, Visualization. **Zhengchun Peng:** Funding acquisition, Resources, Supervision, Writing - review & editing, Conceptualization. **Chenxia Du:** Funding acquisition, Resources, Supervision, Writing - review & editing, Conceptualization. **Bin Zhang:** Data curation, Writing - original draft, Funding acquisition, Resources, Supervision, Writing - review & editing, Conceptualization.

Acknowledgements

This work was supported by the National Natural Science Foundation of China (NSFC) (No. 21601156, 21371154), the Department of Education of Guangdong Province (2016KZDXM005) and the Science and Technology Innovation Council of Shenzhen (KQTD20170810105439418).

Appendix A. Supplementary data

Supplementary data to this article can be found online at <https://doi.org/10.1016/j.dyepig.2020.108487>.

References

- [1] Liu Y, Yiu S-C, Ho C-L, Wong W-Y. Recent advances in copper complexes for electrical/light energy conversion. *Coord Chem Rev* 2018;375:514–57.
- [2] Zhang Y, Schulz M, Wächter M, Kamahl M, Dietzek B. Heteroleptic diimine–diphosphine Cu(I) complexes as an alternative towards noble-metal based photosensitizers: design strategies, photophysical properties and perspective applications. *Coord Chem Rev* 2018;356:127–46.
- [3] Romanov AS, Jones STE, Gu Q, Conaghan PJ, Drummond BH, Feng J, et al. Carbene metal amide photoemitters: tailoring conformationally flexible amides for full color range emissions including white-emitting OLED. *Chem Sci* 2020;11(2): 435–46.

- [4] Hamze R, Shi S, Kapper SC, Muthiah Ravinson DS, Estergreen L, Jung M-C, et al. "Quick-Silver" from a systematic study of highly luminescent, two-coordinate, d10 coinage metal complexes. *J Am Chem Soc* 2019;141(21):8616–26.
- [5] Shi Y, Liu X, Shan Y, Zhang X, Kong W, Lu Y, et al. Naked-eye repeatable off-on-off and on-off-on switching luminescence of copper(I)-1H-imidazo[4,5-f][1,10]phenanthroline complexes with reversible acid–base responses. *Dalton Trans* 2019;48(7):2430–41.
- [6] Xu Y, Shen K, Mao S, Shi X, Wu H, Fan X. Mono- and tetranuclear copper(I) complexes with N-heterocyclic chelating and triphenylphosphine ligands: crystal structures, luminescent and heterogeneous catalytic properties. *Appl Organomet Chem* 2018;32(2):e4041.
- [7] Liu G-N, Zhao R-Y, Xu R-D, Zhang X, Tang X-N, Dan Q-J, et al. A novel tetranuclear copper(I) iodide metal–organic cluster [Cu4I4(ligand)5] with highly selective luminescence detection of antibiotic. *Cryst Growth Des* 2018;18(9):5441–8.
- [8] Tao X-D, Chai W-X, Song L, Wei Q-H, Shi H-S, Qin L-S. Two luminescent pseudopolymorphic cuprous complexes with different optical properties: synthesis, characterization and TD-DFT calculations. *Polyhedron* 2018;144:36–43.
- [9] Wang Z, Zheng C, Wang W, Xu C, Ji B, Zhang X. Synthesis, structure, and photophysical properties of two four-coordinate CuI–NHC complexes with efficient delayed fluorescence. *Inorg Chem* 2016;55(5):2157–64.
- [10] Strel'nik ID, Dayanova IR, Kolesnikov IE, Fayzullin RR, Litvinov IA, Samigullina AI, et al. The assembly of unique hexanuclear copper(I) complexes with effective white luminescence. *Inorg Chem* 2019;58(2):1048–57.
- [11] Musina EI, Shamsieva AV, Strel'nik ID, Gerasimova TP, Krivolapov DB, Kolesnikov IE, et al. Synthesis of novel pyridyl containing phospholanes and their polynuclear luminescent copper(I) complexes. *Dalton Trans* 2016;45(5):2250–60.
- [12] Hamze R, Peltier JL, Sylvainson D, Jung M, Cardenas J, Haiges R, et al. Eliminating nonradiative decay in Cu(I) emitters: >99% quantum efficiency and microsecond lifetime. *Science* 2019;363(6427):601.
- [13] Meng X, Bai R, Wang X, Pan F, He L. Red to blue emitting cationic iridium complexes with 2-phenyl-4-dimethylaminopyridine as the cyclometalating ligand: synthesis, characterization and electroluminescent devices. *Dyes Pigments* 2019;165:458–66.
- [14] Huang J, Liu Z, Chen H, Zhang H, Zhang H, Liu C, et al. formation of heterobinuclear Pt(II)-M(II) complexes based on (2-(1H-Tetrazol-5-yl)phenyl)diphenylphosphine oxide for superior phosphorescence of monomers. *Inorg Chem* 2019;58(7):4253–61.
- [15] Zhao Y, Van Y, Wang D, Li L, Qiu P. Polymer immobilization effect on excited state of emitting copper complex: synthesis, characterization and performance improvement. *J Mol Struct* 2019;1181:171–8.
- [16] Ravaro LP, Mafud AC, Li Z, Reinheimer E, Simone CA, Mascarenhas YP, et al. New emissive mononuclear copper (I) complex: structural and photophysical characterization focusing on solvatochromism, rigidochromism and oxygen sensing in mesoporous solid matrix. *Dyes Pigments* 2018;159:464–70.
- [17] Zhang Q, Chen J, Wu X-Y, Chen X-L, Yu R, Lu C-Z. Outstanding blue delayed fluorescence and significant stability of cuprous complexes with functional pyridine-pyrazolate diimine ligands. *Dalton Trans* 2015;44(15):6706–10.
- [18] Chai W, Hong M, Song L, Jia G, Shi H, Guo J, et al. Three reversible polymorphic copper(I) complexes triggered by ligand conformation: insights into polymorphic crystal habit and luminescent properties. *Inorg Chem* 2015;54(9):4200–7.
- [19] Yang L, Xu X, Zhang P, Chen M, Chen G, Zheng Y, et al. Photophysical properties and stability of binuclear emissive Copper(I) complexes Co-deposited with CuX (X = Cl, Br, I) and aza-9,9'-spirobifluorenes. *Dyes Pigments* 2019;161:296–302.
- [20] Kobayashi A, Fujii M, Shigeta Y, Yoshida M, Kato M. Quantitative solvent-free thermal synthesis of luminescent Cu(I) coordination polymers. *Inorg Chem* 2019;58(7):4456–64.
- [21] Huitorel B, Utrera-Melero R, Massuyeau F, Mevelec J-Y, Baptiste B, Polian A, et al. Luminescence mechanochromism of copper iodide clusters: a rational investigation. *Dalton Trans* 2019;48(22):7899–909.
- [22] Evariste S, Khalil AM, Moussa ME, Chan AK-W, Hong EY-H, Wong H-L, et al. Adaptive coordination-driven supramolecular syntheses toward new polynuclear Cu(I) luminescent assemblies. *J Am Chem Soc* 2018;140(39):12521–6.
- [23] Chen X-L, Yu R, Wu X-Y, Liang D, Jia J-H, Lu C-Z. A strongly greenish-blue-emitting Cu4Cl4 cluster with an efficient spin-orbit coupling (SOC): fast phosphorescence versus thermally activated delayed fluorescence. *Chem Commun* 2016;52(37):6288–91.
- [24] Song Y-L, Jiao B-J, Liu C-M, Peng X-L, Wang M-M, Yang Y, et al. Synthesis, structures and luminescent properties of red emissive neutral copper(I) complexes with bisphosphino-substituted benzimidazole. *Inorg Chem Commun* 2020;112:107689.
- [25] Zhang Q, Zhou Q, Cheng Y, Wang L, Ma D, Jing X, et al. Highly efficient green phosphorescent organic light-emitting diodes based on CuI complexes. *Adv Mater* 2004;16(5):432–6.
- [26] Nitsch J, Kleeberg C, Frohlich R, Steffen A. Luminescent copper(I) halide and pseudohalide phenanthroline complexes revisited: simple structures, complicated excited state behavior. *Dalton Trans* 2015;44(15):6944–60.
- [27] Manbeck GF, Brennessel WW, Eisenberg R. Photoluminescent copper(I) complexes with amido-triazolato ligands. *Inorg Chem* 2011;50(8):3431–41.
- [28] Iwamura M, Watanabe H, Ishii K, Takeuchi S, Tahara T. Coherent nuclear dynamics in ultrafast photoinduced structural change of bis(diimine)copper(I) complex. *J Am Chem Soc* 2011;133(20):7728–36.
- [29] Chen LX, Shaw GB, Novozhilova I, Liu T, Jennings G, Attenkofer K, et al. MLCT state structure and dynamics of a copper(I) diimine complex characterized by Pump–Probe X-ray and laser spectroscopies and DFT calculations. *J Am Chem Soc* 2003;125(23):7022–34.
- [30] Mohankumar M, Holler M, Meichsner E, Nierengarten J-F, Niess F, Sauvage J-P, et al. Heteroleptic copper(I) pseudorotaxanes incorporating macrocyclic phenanthroline ligands of different sizes. *J Am Chem Soc* 2018;140(6):2336–47.
- [31] Osawa M, Kawata I, Ishii R, Igawa S, Hashimoto M, Hoshino M. Application of neutral d10 coinage metal complexes with an anionic bidentate ligand in delayed fluorescence-type organic light-emitting diodes. *J Mater Chem C* 2013;1(28):4375–83.
- [32] Cuttell DG, Kuang S-M, Fanwick PE, McMillin DR, Walton RA. Simple Cu(I) complexes with unprecedented excited-state lifetimes. *J Am Chem Soc* 2002;124(1):6–7.
- [33] Mondal R, Lozada IB, Davis RL, Williams JAG, Herbert DE. Exploiting synergy between ligand design and counterion interactions to boost room temperature phosphorescence from Cu(I) compounds. *J Mater Chem C* 2019;7(13):3772–8.
- [34] Liu L-P, Li Q, Xiang S-P, Liu L, Zhong X-X, Liang C, et al. Near-saturated red emitters: four-coordinate copper(I) halide complexes containing 8-(diphenylphosphino)quinoline and 1-(diphenylphosphino)naphthalene ligands. *Dalton Trans* 2018;47(28):9294–302.
- [35] Mondal R, Lozada IB, Davis RL, Williams JAG, Herbert DE. Site-selective benzannulation of N-heterocycles in bidentate ligands leads to blue-shifted emission from [P(N)Cu]2(μ-X)2 dimers. *Inorg Chem* 2018;57(9):4966–78.
- [36] Harkins SB, Peters JC. A highly emissive Cu2N2 diamond core complex supported by a [PNP]-ligand. *J Am Chem Soc* 2005;127(7):2030–1.
- [37] Yersin H, Czerwieniec R, Shafikov MZ, Suleymanova AF. TADF material design: photophysical background and case studies focusing on CuI and AgI complexes. *ChemPhysChem* 2017;18(24):3508–35.
- [38] Hsu C-W, Lin C-C, Chung M-W, Chi Y, Lee G-H, Chou P-T, et al. Systematic investigation of the metal-structure–photophysics relationship of emissive d10-complexes of group 11 elements: the prospect of application in organic light emitting devices. *J Am Chem Soc* 2011;133(31):12085–99.
- [39] Schinabeck A, Chen J, Kang L, Teng T, Homeier HHH, Suleymanova AF, et al. Symmetry-based design strategy for unprecedentedly fast decaying thermally activated delayed fluorescence (TADF). Application to dinuclear Cu(I) compounds. *Chem Mater* 2019;31(12):4392–404.
- [40] Leitl MJ, Küchle F-R, Mayer HA, Wesemann L, Yersin H. Brightly blue and green emitting Cu(I) dimers for singlet harvesting in OLEDs. *J Phys Chem* 2013;117(46):11823–36.
- [41] Cariati E, Lucenti E, Botta C, Giovannella U, Marinotto D, Righetto S. Cu(I) hybrid inorganic–organic materials with intriguing stimuli responsive and optoelectronic properties. *Coord Chem Rev* 2016;306(2):566–614.
- [42] Yam VW-W, Au VK-M, Leung SY-L. Light-emitting self-assembled materials based on d8 and d10 transition metal complexes. *Chem Rev* 2015;115(15):7589–728.
- [43] Shi H, Zou L, Huang K, Wang H, Sun C, Wang S, et al. A highly efficient red metal-free organic phosphor for time-resolved luminescence imaging and photodynamic therapy. *ACS Appl Mater Interfaces* 2019;11(20):18103–10.
- [44] Tang Z, Zhu J, Pan S, Wang Z, Zheng Y, Chen G, et al. Synthesis of carboline-based host materials for forming copper(I) complexes as emitters: a promising strategy for achieving high-efficiency and low-cost phosphorescent organic light-emitting diodes. *Dyes Pigments* 2018;149:387–92.
- [45] Zhang Q, Chen X-L, Chen J, Wu X-Y, Yu R, Lu C-Z. Photo- and electro-luminescence of four cuprous complexes with sterically demanding and hole transmitting diimine ligands. *Dalton Trans* 2015;44(21):10022–9.
- [46] Sun Y, Lemaur V, Beltrán JI, Cornil J, Huang J, Zhu J, et al. Neutral mononuclear copper(I) complexes: synthesis, crystal structures, and photophysical properties. *Inorg Chem* 2016;55(12):5845–52.
- [47] McCormick T, Jia W-L, Wang S. Phosphorescent Cu(I) complexes of 2-(2'-pyridyl)benzimidazolyl)benzene: impact of phosphine ancillary ligands on electronic and photophysical properties of the Cu(I) complexes. *Inorg Chem* 2006;45(1):147–55.
- [48] Clegg W, Elsegood MRJ, Errington RJ, Fisher GA, Norman NC. Structure of Bibr2Ph: a solid-state architecture involving secondary bonding and π–π interactions. *J Mater Chem* 1994;4(6):891–3.
- [49] Shi S, Jung MC, Coburn C, Tadler A, Sylvainson MRD, Djurovich PI, et al. Highly efficient photo- and electroluminescence from two-coordinate Cu(I) complexes featuring nonconventional N-heterocyclic carbenes. *J Am Chem Soc* 2019;141(8):3576–88.
- [50] Lin L, Chen D-H, Yu R, Chen X-L, Zhu W-J, Liang D, et al. Photo- and electro-luminescence of three TADF binuclear Cu(I) complexes with functional tetraimine ligands. *J Mater Chem C* 2017;5(18):4495–504.
- [51] Liu R, Shu M, Hu J, Zhu S, Shi H, Zhu H. Star-shaped D-π-A compounds with a 1,3,5-triazine core and N-aryl chromophore substituted fluorene arms: synthesis, aggregation induced emission and two-photon absorption. *Dyes Pigments* 2017;137:174–81.
- [52] Neshat A, Aghakhanpour RB, Mastrorilli P, Todisco S, Molani F, Wojtczak A. Dinuclear and tetranuclear copper(I) iodide complexes with P and P'N donor ligands: structural and photoluminescence studies. *Polyhedron* 2018;154:217–28.
- [53] Kobayashi A, Yoshida Y, Yoshida M, Kato M. Mechanochromic switching between delayed fluorescence and phosphorescence of luminescent coordination polymers composed of dinuclear copper(I) iodide rhombic cores. *Chem Eur J* 2018;24(55):14750–9.
- [54] Zhang Q, Komino T, Huang S, Matsunami S, Goushi K, Adachi C. Triplet exciton confinement in green organic light-emitting diodes containing luminescent charge-transfer Cu(I) complexes. *Adv Funct Mater* 2012;22(11):2327–36.
- [55] Miller AJM, Dempsey JL, Peters JC. Long-lived and efficient emission from mononuclear amidophosphine complexes of copper. *Inorg Chem* 2007;46(18):7244–6.

- [56] Krylova VA, Djurovich PI, Whited MT, Thompson ME. Synthesis and characterization of phosphorescent three-coordinate Cu(I)-NHC complexes. *Chem Commun* 2010;46(36).
- [57] Jiao B, Wang J, Huang J, Cao M, Liu C, Yin G, et al. Design and synthesis of stable cuprous complexes bearing P^AN-type ligands for vapor-deposited organic light-emitting device. *Org Electron* 2019;64:158–65.
- [58] Osawa M. Highly efficient blue-green delayed fluorescence from copper(I) thiolate complexes: luminescence color alteration by orientation change of the aryl ring. *Chem Commun* 2014;50(15):1801–3.
- [59] Pillay MN, Liao J-H, Liu CW, van Zyl WE. Aqueous route to stable luminescent tetranuclear copper(I) dithiophosphonate clusters. *Inorg Chem* 2019;58(10):7099–106.
- [60] Yang X, Yan X, Guo H, Liu B, Zhao J, Zhou G, et al. Charged dinuclear Cu(I) complexes for solution-processed single-emitter warm white organic light-emitting devices. *Dyes Pigments* 2017;143:151–64.
- [61] CrysAlisPro, Agilent technologies, Version 11713628.
- [62] Sheldrick G. A short history of SHELX. *Acta Crystallogr A: Found Crystallogr* 2008;64(1):112–22.
- [63] Do V, Bl J, Gr J, Hja K, Horst P. Olex2: A complete structure solution, refinement and analysis program. *J Appl Crystallogr* 2009;42(2):339–41.
- [64] Sheldrick G. Crystal structure refinement with SHELXL. *Acta Crystallogr C* 2015;71(1):3–8.
- [65] Frisch MJ, Trucks GW, Schlegel HB, Scuseria GE, Robb MA, Cheeseman JR, et al. Gaussian 09, revision D.01. Gaussian 09, revision D01 Gaussian. Wallingford CT: Inc.; 2013. 2013.
- [66] Chandra R, Dutta A, Manna AK, Rout K, Mondal J, Patra GK. Halide bridged novel ternary copper(I) complexes with bis imino-quinolonyl ligand and triphenylphosphine: synthesis, structure, luminescence, electrochemistry and theoretical studies. *Inorg Chim Acta* 2019;496:119042.
- [67] Becke AD. Density-functional thermochemistry. III. The role of exact exchange. *J Chem Phys* 1993;98(7):5648–52.
- [68] Lee C, Yang W, Parr RG. Development of the Colle-Salvetti correlation-energy formula into a functional of the electron density. *Phys Rev B* 1988;37(2):785–9.
- [69] Runge E, Gross EKV. Density-functional theory for time-dependent systems. *Phys Rev Lett* 1984;52(12):997–1000.
- [70] Chai C, Xu S, Wang J, Zhao F, Xia H, Wang Y. Synthesis, photophysical properties and DFT studies of the pyridine-imidazole (PyIm) Cu(I) complexes: impact of the pyridine ring functionalized by different substituents. *Inorg Chim Acta* 2019;488:34–40.
- [71] Hay PJ, Wadt WR. Ab initio effective core potentials for molecular calculations. Potentials for K to Au including the outermost core orbitals. *J Chem Phys* 1985;82(1):299–310.
- [72] Hay PJ, Wadt WR. Ab initio effective core potentials for molecular calculations. Potentials for the transition metal atoms Sc to Hg. *J Chem Phys* 1985;82(1):270–83.
- [73] Yu Y, Ma L, Feng Z, Liu B, Zhou H, Qin H, et al. Strategy for achieving efficient electroluminescence with reduced efficiency roll-off: enhancement of hot excitons spin mixing and restriction of internal conversion by twisted structure regulation using an anthracene derivative. *J Mater Chem C* 2019;7(19):5604–14.
- [74] Gao F, Du R, Han C, Zhang J, Wei Y, Lu G, et al. High-efficiency blue thermally activated delayed fluorescence from donor–acceptor–donor systems via the through-space conjugation effect. *Chem Sci* 2019;10(21):5556–67.
- [75] Tian L, Feiwu C. Multiwfn: a multifunctional wavefunction analyzer. *J Comput Chem* 2012;33(5):580–92.